Comparison of Welding Residual Stresses of Hybrid Laser-Arc Welding and Submerged Arc Welding in Offshore Steel Structures

Andreassen, Michael Joachim; Yu, Zhenzhen; Liu, Stephen; Guerrero-Mata, Martha Patricia

Published in:
Proceedings of the 10th International Conference on Trends in Welding Research

Publication date:
2016

Document Version
Publisher's PDF, also known as Version of record

Comparison of Welding Residual Stresses of Hybrid Laser-Arc Welding and Submerged Arc Welding in Offshore Steel Structures

Michael Joachim Andreassen
Technical University of Denmark, Department of Civil Engineering, DK-2800 Kgs. Lyngby, Denmark
mican@byg.dtu.dk, +(45) 45 25 18 14

Zhenzhen Yu, Stephen Liu
Colorado School of Mines, Department of Metallurgical and Materials Engineering, Golden, CO 80401, USA
zyu@mines.edu, +(1) 303 273-3798, sliu@mines.edu,+(1) 303 273-3796

Martha Patricia Guerrero-Mata
Universidad Autonoma de Nuevo Leon, Facultad de Ingenieria Mecanica y Electrica, San Nicolas de los Garza, N.L. 66455, Mexico
martha.guerreromt@uanl.edu.mx, +(52) 81 8329 4020

Abstract
In the offshore industry, welding-induced distortion and tensile residual stresses have become a major concern in relation to the structural integrity of a welded structure. Particularly, the continuous increase in size of welded plates and joints needs special attention concerning welding induced residual stresses. These stresses have a negative impact on the integrity of the welded joint as they promote distortion, reduce fatigue life, and contribute to corrosion cracking and premature failure in the weld components.
This paper deals with the influence and impact of welding method on the welding induced residual stresses. It is also investigated whether the assumption of residual stresses up to yield strength magnitude are present in welded structures as stated in the design guidelines. The fatigue strength for welded joints is based on this assumption.
The two welding methods investigated are hybrid laser-arc welding (HLAW) and submerged arc welding (SAW). Both welding methods are applied for a full penetration butt-weld of 10 mm thick plates made of thermomechanically hot-rolled, low-carbon, fine-grain S355ML grade steel used in offshore steel structures.
The welding residual stress state is investigated by means of computational welding mechanics, experiments, and in accordance with existing production procedures to determine the real distribution and magnitude of the residual stresses. The experimental validation of the FE simulations includes temperature and hole-drilling measurements.

1 Introduction
Supersize monopiles used for offshore wind turbine support structures are being developed and have already been installed on several offshore wind farms. The demand for fabrication of monopiles with large wall thicknesses is high. However, the implications on design and especially the joining of cans by circumferential welding with these wall thicknesses are not yet fully understood. Particularly, the welding induced residual stresses need special attention. The stresses have a negative impact on the integrity of the welded joint as they promote distortion, reduce fatigue life, and contribute to corrosion cracking and premature failure in the weld components. Research within the field of welding residual stresses is important as the size of structures and welds are rapidly increasing. The steel fabricators raise the demands, as deeper foundations are needed due to design requirements.
This paper deals with the influence and impact of welding method on the welding induced residual stresses. In this relation, it is also investigated whether the assumption that residual stresses up to yield strength magnitude are present in welded structures as stated in the design guidelines, [1,2,3]. The fatigue strength for welded joints is based on this assumption. The two welding methods investigated are submerged arc-welding (SAW) and hybrid laser-arc welding (HLAW). Both welding methods are applied for a full penetration butt-weld of 10 mm thick plates produced of thermomechanically hot-rolled, low-carbon, fine-grain S355ML grade steel.
By investigating the welding residual stresses through numerical simulations, experiments and in accordance with existing production procedures, an optimization of the fatigue design is expected, leading to a more efficient and improved design. In this context, this research is expected to benefit the offshore industry by leading to an improved design which consequently can be included in present norms and standards. Further, it will optimize the correlation between numerical simulations and physical models.
3D FE models are very CPU time consuming. Thus, this paper deals with a steel plate thickness of 10 mm which makes it easier to adjust and optimize the FE models. The experiences gained from this model will then form the basis of the modelling technique utilized for the thicker plates used for the construction of monopiles.

2 Material Tests and Results

The material used for the experiments is thermomechanically hot-rolled, low-carbon, fine-grain structural steel of grade S355ML in accordance with the European Standard, [4]. This steel grade is widely used for offshore structures and possesses excellent weldability. It has a lower carbon content than grade S355NL steel (normalized and rolled) which lowers the cold cracking tendency and increases the toughness in the HAZ. The increased performance against cold cracking makes it possible to reduce the preheating, which leads to cost reduction in terms of reduced fabrication time and energy savings. The chemical composition of grade S355ML steel is shown in Table 1.

Table. 1: Chemical composition (in wt. pct.) of S355ML steel.

C %	Si %	Mn %	P %	S %	Al %	Cr %	Ni %	Mo %	Cu %	V %	Nb %	Ti %	N %	B %	Cae %
.082	.332	1.37	.01	.0005	.045	.024	.012	.004	.016	.003	.027	.014	.0052	.0002	.32

Experiments include the determination of material properties such as elastic modulus, yield stress and ultimate strength. Thus, 25 room and high temperature monotonic tensile tests have been performed in the temperature range from 20°C to 1000°C. The tests followed the European tensile testing standards for metallic material, [5,6]. Fig. 1 shows the tensile test setup.

Fig. 1: High temperature monotonic tensile test setup.

An MTS 312.31, 250 kN, universal testing machine was used. Displacement and load were logged by the testing machine and output was a stress-strain curve. An Instron, type 2620-601, extensometer with a range of 50 mm was used on the specimens to measure the displacement over an initial gauge distance, which was used to determine the modulus of elasticity.

Table. 2: Mechanical properties of S355ML steel.

Temp. (°C)	20	100	200	300	400	500	600	700	800	1000
E (MPa) x 10^5	2.18	2.03	2.15	1.86	1.06	1.54	0.91	0.53	0.39	0.14
f_y (MPa)	404	380	366	325	244	210	132	104	34	22
f_u (MPa)	601	535	556	597	521	372	179	121	46	39

Table 2 shows the mean values of elastic modulus, yield stress and ultimate strength given in the temperature range from 20°C to 1000°C. It is seen how the elastic modulus, yield stress and ultimate strength decreases as the temperature increases.

3 Welding Experiments

The following three subsections contain a brief description of the welding experiments. The first subsection concerns the test weld specimens while the second and third subsections concern the submerged arc welding process and the hybrid laser-arc welding process, respectively.

3.1 Test Weld Specimens

The geometry of the welding application comprises a full penetration, one-sided butt-weld joining two identical plates, each with a dimension of 480 × 240 × 10 mm. The perpendicular edges have been prepared by water jet cutting and the weld grooves by flame cutting. The weld grooves are different for the two welding methods and will thus be described in the following two subsections. Fig. 2 shows an isometric view of the test plate geometry.

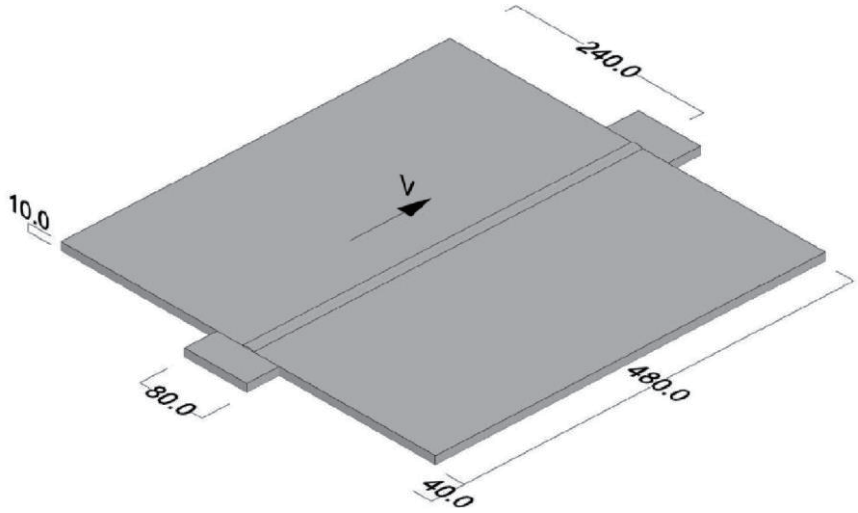

Fig. 2: Isometric view of geometry.

The two main plates have been constrained (tack-welded) by a run-on and a run-off plate of 80 × 40 × 10 mm at each end of the weld plate.

3.2 Submerged Arc Welding Experiments

The Submerged Arc Welding (SAW) butt-weld consists of two weld-passes; a root-pass and a cover-pass, which have an interpass time of 940 seconds. The weld geometry comprises a bezel angle of 35°, a nose height of 3.0 mm and a nose opening of 0.0 mm. An underlying bench supports the plates in the vertical downward direction.

Table 3: Welding procedure specifications for SAW.

Pass	AC/DC	Efficiency	Wire (mm)	Current (A)	Voltage (V)	Travel Speed (cm/min)/(mm/s)	Heat input (kJ/cm)
SAW 1	DC+	0.98	4	535	27.3	36/6	24
SAW 2	DC+	0.98	4	535	27.3	36/6	24

Table 4: Properties of filler wire and flux powder.

	C (%)	Si (%)	Mn (%)	P (%)	S (%)	Cu (%)	f_y (MPa)	f_u (MPa)	El. (%)	Impact Energy (J) T(°C)
OK Autrod 12.22/L	0.1	0.2	1.0	0.018	0.018	0.25	–	–	–	–
With OK flux 10.71/72	0.08	0.5	1.5	–	–	–	440	530	30	50 −40

Table 3 presents the welding procedure specification and the filler wire and flux powder properties are given in Table 4.

3.3 Hybrid Laser-Arc Welding Experiments

The Hybrid Laser-Arc Welding (HLAW) consists of two passes; first, a Metal Active Gas (MAG) weld pass from the bottom side of the plates followed by a Hybrid Laser-Arc pass from the top side. The MAG pass is performed in order to reduce the risk of laser beam penetration between the two plates. The weld geometry comprises a bezel angle of 15°, a nose height of 5.0 mm and a nose opening of 0.0 mm. The groove angle is only used for the MAG pass. Consequently, the HLAW pass is performed from the opposite side without any groove angle. An underlying bench supports the plates in the vertical downward direction.

Table 5: Welding procedure specifications for the root pass (MAG) and cover pass (HLAW).

Pass	Travel Speed (m/min)	Wire Diameter (mm)	Stick out (mm)	MAG Current (A)	MAG Voltage (V)	Laser (kW)	Weld Speed (mm/min)
1 (MAG)	9.5	1.2	25	310	33.5	–	650
2 (HLAW)	9.5	1.2	25	310	25	8	1000

Table 6: Chemical composition (in wt. pct.) and mechanical properties of the wire OK Autrod 12.51 and weld.

	C (%)	Si (%)	Mn (%)	P (%)	S (%)	f_y (MPa)	f_u (MPa)	A4−A5 (%)	Z	Impact Energy (J)	Impact Energy T (°C)
Min	0.06	0.80	1.40	–	–	–	–	–	–	–	–
Max	0.14	1.00	1.60	0.025	0.025	–	–	–	–	–	–
As welded	0.10	0.72	1.11	0.013	0.012	470	560	26	68	130, 90, 70	20, 20, 30

Table 5 provides the welding procedure specifications and Table 6 lists the chemical composition and mechanical properties of the weld.

4 FE Model

Experiments normally form the basis for developing welding procedures contained in a Welding Procedure Specification (WPS). This methodology also implies that the basis for WPS is observations of e.g. joint integrity, absence of defects, microstructure and mechanical testing [7]. With increasing computational power over the last decades, one of the significant tools applied for additional design considerations is the finite element analysis. FEA is rarely used in the process of developing welding procedures; however, it is expected that simulations can be used to complement the experimental procedures for preparing a WPS since the resulting residual stress and distortion can then be considered when comparing different welding procedures. Furthermore, simulations are useful in designing the manufacturing process as well as the manufactured component itself. A coupled 3D FE model simulates the present welding process and analyses the residual stress state. The 3D model includes the transient heat transfer along with the material properties at different temperatures. It was decided to consider the coupling of the heat transfer and the stress analysis as one-way coupled, in order to reduce the computational costs considerably. The commercial FE program Abaqus models the welding process using a computer capacity of 8 CPUs and 128 GB RAM. Fig. 3 lists the model geometry and the used mesh configuration.

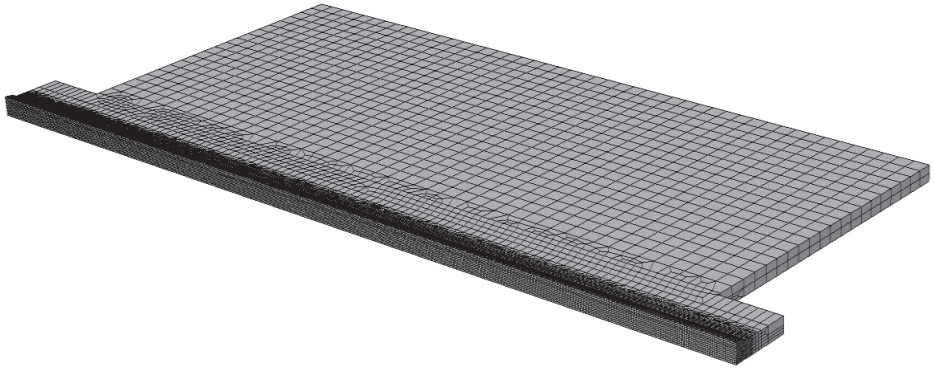

Fig. 3: Model geometry and mesh configuration.

Isotropic models have been used and the Goldak double ellipsoid heat source model has been applied by using the Dflux subroutine.

5 Temperature Distribution

Temperature measurements during welding monitor in-situ the temperature evolution in the plates. The measurements verify the FE model and guide the mapping of the residual stresses in the hole drilling experiments. Fig. 4 shows the heat flow pattern from the FE models for both the submerged arc welding and the hybrid laser-arc welding. It is noticed that the SAW has a wider temperature distribution than the HLAW for both the transverse and the longitudinal direction, and that the maximum temperature is highest for the HLAW.

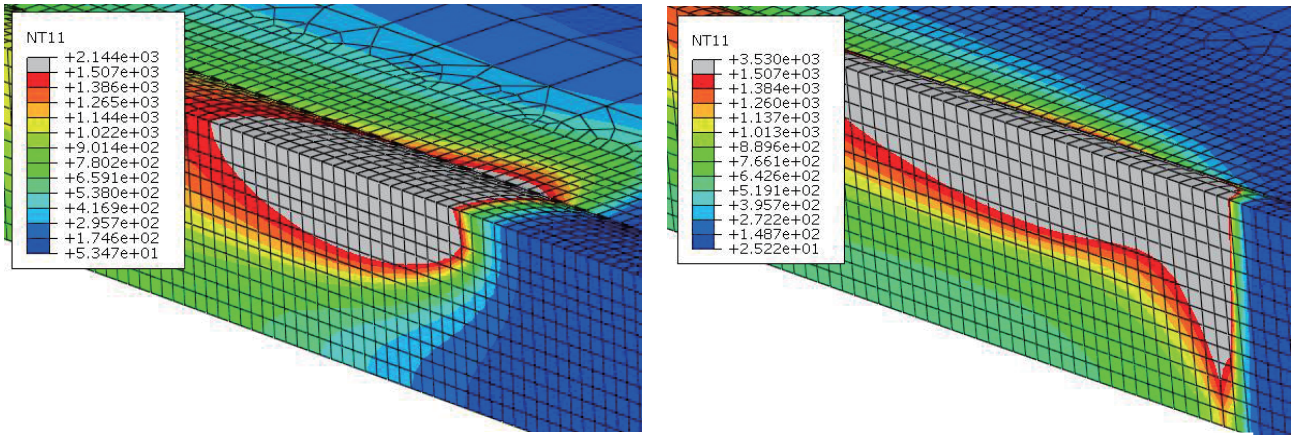

Fig. 4: Heat flow pattern calculated with the FE models for submerged arc welding (left) and hybrid laser-arc welding (right). All temp. in ℃.

In the analysis of the thermal gradients from the welding procedure, it is desired to have measurements as close as possible to the weld pool due to buildup of residual stresses, which are highly influenced by the peak temperatures caused by the transient heat source. The distance between the thermocouples is therefore shortest close to the weld. The position of the thermocouples is in the middle of the plate corresponding to 5 mm below the surface. The thermocouples are type "K" MI with a probe-diameter of 1.5 mm and a length of 150 mm. A HP, model 34970A, data logger acquired the thermocouple data. The temperature measurements have an interval of 1 second.
For the SAW temperature measurements the first pass reached a maximum temperature of 598°C and the second pass a maximum temperature of 679°C at a distance of 10 mm from the center of the weld. The second pass was expected to have a higher maximum temperature since it started at an initial temperature of 75°C compared with the room temperature for the first pass.
For the HLAW experiments, the MAG welding pass reached a maximum temperature of 324°C and for the HLAW the maximum temperature was 395°C, both at a distance of 10 mm from the center of the weld.
In relation to the temperature distribution, the SAW weld is expected to result in a wider region of welding residual stresses compared to the HLAW because of the wider temperature distribution reached.

6 Residual Stress Distribution

Hole-drilling measurements were performed to map the stress distribution as a function of the distance away from the welds produced with the two different welding methods. The hole-drilling measurements as well as the temperature measurements validated the FE model. Prior to the hole-drilling measurements the surface was prepared by grinding to remove the mill scale for proper bonding of the strain gauges. Micro-measurements RS-200 hole-drilling equipment and software as well as standardized hole-drilling strain gauge rosettes E837 type A, 031RE and 062RE, with a maximum stress data depth of 0.5 mm and 1.0 mm, respectively, was used. As the hole-drilling method measures the residual stresses close to the surface, the comparison between the experimental and FE model predictions is limited with respect to the vertical distance from the surface. Moreover, it is not possible to measure the stresses in the weld by using the hole-drilling method, as the strain gauges require a flat and smooth surface. It is anticipated that such a weld surface would also change the residual stresses in the weld. These concerns means that the maximum residual stresses measured by the FE model and the hole drilling method cannot be directly compared. However, it is possible to measure and compare the stresses close to the surface at a horizontal distance of 4 mm from the weld fusion line and further away. Fig. 5 compares the maximum longitudinal residual stress distribution for both welding methods. The distribution is from the plate centerline cross section. The weld beat width is 10 mm for the SAW and 5 mm for the HLAW. In relation to the mentioned temperature distribution, which are widest for the SAW, hence it is expected that the SAW will introduce a wider region and a greater amount of welding residual stresses compared to the HLAW.

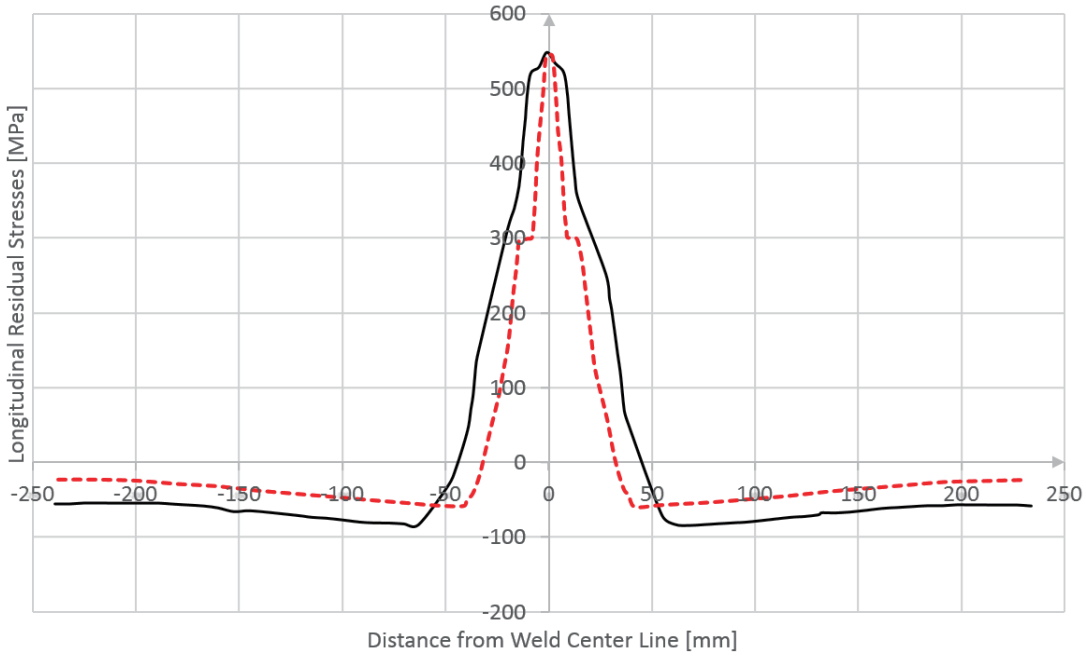

Fig. 5: Longitudinal welding residual stresses for SAW (solid line) and HLAW (dotted line).

Fig. 5 depicts a wider stress distribution for the SAW than for the HLAW. However, both welding methods result in approximately the same maximum longitudinal residual stress value. The maximum FEM longitudinal welding residual stresses calculated in the middle of the cross section are 565 MPa and 562 MPa for SAW and HLAW, respectively. Thus, the maximum residual stresses calculated are approximately the same for the SAW and HLAW; however, the distribution of the stresses is different. The distribution is much wider for the SAW than for the HLAW thus making the total amount of residual stresses larger for the SAW.

7 Conclusions

Two different butt-welds obtained by SAW and HLAW of 10 mm thick steel plates have been analyzed by experiments, FE models and in accordance with existing production procedures. The use of a coupled 3D FE model to simulate both welding processes has shown to be sufficient to map the residual stress distribution. The Goldak double ellipsoid distributed heat source was applied via Dflux subroutine on the 3D model. The developed 3D FE models show good agreement with the experimental measurements of the weldments. The SAW method has a wider distribution of the residual stresses than the HLAW method as well as higher maximum compression residual stresses. However, both welding methods results in approximately the same maximum tensile residual stress value. As the maximum longitudinal stresses are higher than the yield strength for both welding methods an underestimation is found when assuming residual stresses up to yield strength magnitude in welded structures.

Acknowledgments

The authors are grateful to Lindoe Welding Technology for the support provided developing the HLAW testing.

References

[1] Eurocode 3: “Design of steel structures - Part 1-9: Fatigue“. Danish Standard, 2005.
[2] Det Norske Veritas, DNV-OS-J101, Design of Offshore Wind Turbine Structures. DNV, 2010.
[3] J. Krebs, *et al*: Influence of Welding Residual Stresses on Fatigue Design of Welded Joints and Components: IIW Doc. IIW-1805-07; 2007.
[4] DS/EN 10025-4-2004, Hot rolled products of structural steels – Part 4: Technical delivery conditions for thermomechanical rolled weldable fine grain structural steels, 2004.
[5] DS-EN ISO 6892-1-2013 - Metallic material - Tensile testing Part 1: Method of test at room temperature.
[6] DS-EN ISO 6892-2-2013 - Metallic material - Tensile testing Part 2: Method of test at elevated temperature.
[7] L.E. Lindgren: “Finite Element Modeling and Simulation of Welding - Part 1: Increased Complexity”, Journal of Thermal Stresses, Vol. 24, 2001.